Density Functional Study on Molybdacyclobutane and Its Role in Olefin Metathesis

E. Folga and T. Ziegler*

Department of Chemistry, University of Calgary, Calgary, Alberta, Canada T2N 1N4

Received July 31, 1992

A theoretical study has been carried out on the molecular and electronic structure of the metal carbene $L_2Mo(X)CH_2$ (A) as well as the metallacycle $L_2Mo(X)C_3H_6$ (B), with full geometry optimization for X = O, NH and L = Cl, OCH_3, OCF_3. A square-pyramidal (SP) as well as a trigonal-bipyramidal (TBP) conformation was considered for B. The metallacycle B is calculated to be stable with respect to decomposition into A and ethylene. The decomposition energies are calculated in kJ/mol as follows (L, X): SP structures, (Cl, O) 54, (Cl, NH) 43, (OCH_3, O) 66, (OCH_3, NH) 61, (OCF_3, O) 61, (OCF_3, NH) 49; TBP structures, (Cl, O) 21, (Cl, NH) 38, (OCH_3, O) 44, (OCH_3, NH) 57, (OCF_3, O) 44, (OCF_3, NH) 74. The calculated decomposition energies indicate that the SP conformation is more stable than the TBP conformation for $L_2Mo(O)C_3H_6$. The corresponding $L_2Mo(NH)C_3H_6$ system prefers TBP for the electron-withdrawing ligand L = OCF_3 and SP for L = Cl, OCH_3. The formation of B from ethylene and A has a small activation barrier of 10 kJ/mol. A detailed analysis is provided of the process between A and ethylene leading to the two conformations of B. The two paths have a similar transition state where ethylene is interacting weakly with A. The SP conformation is formed by nucleophilic attack of ethylene on the metal followed by a nucleophilic attack of the carbene carbon at the olefin. The TBP conformation is formed by a concerted process in which both nucleophilic attacks take place simultaneously. The $[2_\pi + 2_\pi]$ addition between carbene and olefin is made feasible by nonzero π-to-π^* overlaps and a considerable energy gap between $\pi_{carbene}$ and π_{olefin} with π_{olefin} 4 eV lower in energy.

I. Introduction

Carbene complexes of tungsten and molybdenum are efficient catalysts for the metathesis of olefin (eq 1a).

$$R^1CH{=}CHR^2 + R^3CH{=}CHR^4 \rightarrow R^1CH{=}CHR^3 + R^2CH{=}CHR^4 \quad (1a)$$

Chauvin[1] was the first to suggest that metal carbenes act as catalysts by undergoing a $[2_\pi + 2_\pi]$ cycloaddition reaction with olefin, thus forming the metallacyclobutane **1a**. The subsequent decomposition of the intermediate metallacycle **1a** results in the formation of a new olefin (eq 1b). Chauvin's mechanism is now widely accepted, and several metallacyclobutanes have been isolated and characterized.

$$L_2M(NR)CHR^1 + R^2CH{=}CHR^3 \longrightarrow$$

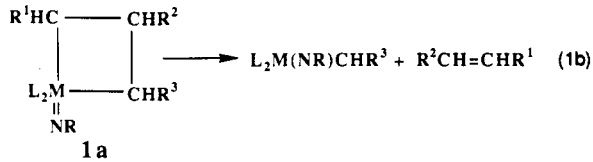

$$\rightarrow L_2M(NR)CHR^3 + R^2CH{=}CHR^1 \quad (1b)$$

1a

Schrock[2] et al. have studied the catalytic activity of $(OR)_2W(NR')CH_2$ and $(OR)_2Mo(NR')CH_2$. They find that alkoxy ligands with bulky and electron-withdrawing substituents enhance the activity of $(OR)_2M(NR')CH_2$, whereas less electron withdrawing R groups such as R = *t*-Bu afford catalysts with little or no activity. Schrock[2] et al. have also carried out detailed investigations on the intermediate metallacycle **1a**. The active metal carbenes with bulky and electron-withdrawing alkoxy groups such as $OCMe(CF_3)_2$ and $OC(CF_3)_2(CF_2CF_2CF_3)$ afford metallacycles with a trigonal-bipyramidal structure (**1b**), whereas the less active carbenes with electron-releasing alkoxy groups give rise to square-pyramidal metallacycles (**1c**). The relation between the electronic properties of the alkoxy group (OR) and the activity of the carbene $(OR)_2M(NR')CH_2$ as well as the conformational preference of the corresponding metallacycle **1a** is not fully understood.[2c]

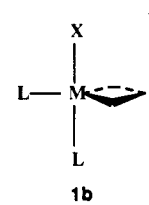

1b

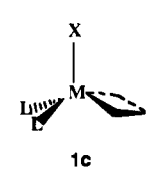

1c

We present here a systematic study on the $[2_\pi + 2_\pi]$ cycloaddition reaction of eq 1b, the key step in olefin metathesis catalyzed by $(L)_2Mo(X)CH_2$. The first objective of our investigation has been to understand why the formally symmetry forbidden $[2_\pi + 2_\pi]$ cycloaddition

(1) Hérisson, J.-L.; Chauvin, Y. *Makromol. Chem.* **1970**, *141*, 161.

(2) (a) Feldman, J.; Davis, W. M.; Schrock, R. R. *Organometallics* **1989**, *8*, 2266. (b) Schrock, R. R.; DePue, R. T.; Feldman, J.; Yap, K. B.; Yang, D. C.; Davis, W. M.; Park, L.; DiMare, M.; Schofield, M.; Anhaus, J.; Walborsky, E.; Evitt, E.; Kruger, C.; Betz, P. *Organometallics* **1990**, *9*, 2262. (c) Feldman, J.; Davis, W. M.; Thomas, J. K.; Schrock, R. R. *Organometallics* **1990**, *9*, 2535. (d) Schrock, R. R. *Acc. Chem. Res.* **1990**, *23*, 158. (e) Schrock, R. R.; Murdzek, J. S.; Bazan, G. C.; Robbins, J.; DiMare, M.; O'Regan, M. *J. Am. Chem. Soc.* **1990**, *112*, 3875. (f) Schrock, R. R.; DePue, R. T.; Feldman, J.; Schaverien, C. J.; Devan, J. C.; Liu, A. H. *J. Am. Chem. Soc.* **1988**, *110*, 1423.

0276-7333/93/2312-0325$04.00/0

reaction in eq 1b is facile whereas the corresponding addition reaction between two olefins, eq 1a, has an insurmountable activation barrier. We shall to this end study the electronic and molecular structures of the catalysts $(L)_2Mo(X)CH_2$ as well as the intermediate **1a**.

The second part of our study is concerned with the influence of the coligand L and the spectator ligand X on the relative stabilities of **1b** and **1c** as well as the ease by which these metallacycles can break up into olefin and the metal carbene $(L)_2Mo(X)CH_2$. Our choice of coligands includes L = Cl as well as the electron-releasing alkoxy group OCH_3 and the electron-withdrawing alkoxy ligand OCF_3. We shall further probe the influence of the spectator ligand X by considering X = O as well as X = NH. Although most of the experimental work has been done using tungsten as the metal center, we feel that molybdenum is a realistic model for our calculations. It displays comparable chemistry and is computationally less demanding.

The up-to-date detailed calculations on related systems have been performed essentially by two groups, both of which have focused on early-transition-metal complexes. Using the EHT method, Hoffmann and co-workers[3] studied $Cp_2TiC_3H_6$, while Rappé and Upton[4a,b] utilized the GVB method to study the $Cl_2TiC_3H_6$ model system. Using the latter method, Rappé[4c,d] and Goddard have also calculated the reactivities of certain Cr, W, and Mo dichloride methylidene systems toward olefins in studies on olefin metathesis and olefin polymerization. Cundari and Gordon[5] have more recently provided a theoretical analysis of metal carbenes used in olefin metathesis.

II. Computational Details

The reported calculations were all carried out by utilizing the HFS-LCAO program system A-MOL, developed by Baerends et al.[6,7] and vectorized by Ravenek.[8] The numerical integration procedure applied for the calculations was developed by Boerrigter[9] et al. The electronic configurations of the molecular systems were described by an uncontracted triple-ζ STO basis set[10] on molybdenum for 4s, 4p, 4d, 5s, and 5p as well as a double-ζ STO basis set[11] on carbon (2s, 2p), chlorine (3s, 3p), oxygen (2s, 2p), and hydrogen (1s). Hydrogens, oxygens, and carbons were given an extra polarization function: $3d_C$ (ζ_{3d} = 2.5); $3d_O$ (ζ_{3d} = 2.0); $2p_H$ (ζ_{2p} = 2.0). The $1s^22s^22p^63s^23p^63d^{10}$ configuration on molybdenum and the $1s^2$ configuration on carbon and oxygen as well as the $1s^22s^22p^6$ configuration on chlorine were assigned to the core and treated by the frozen-core approximation. A set of auxiliary[12] s, p, d, f, and g STO functions, centered on all nuclei, was used in order to fit the molecular density and present Coulomb and exchange potentials accurately in each SCF cycle. Energy differences were calculated by including the local exchange-correlation potential by Vosko[13] et al. with Becke's[14] nonlocal exchange corrections and Perdew's[15] nonlocal correlation correction. Geometries were optimized without including nonlocal corrections. A recent investigation[16f] has shown that density functional based calculations with and without nonlocal corrections afford quite similar reaction profiles for singlet surfaces as studied here. The application of approximate density functional theory to organometallic chemistry has been reviewed recently.[16a,17]

III. Results and Discussion

The Carbene. We shall begin our discussion on the metathesis reaction in eq 1b by providing an analysis of the electronic and molecular structure of the reacting carbene. In particular, in our analysis of the electronic structure we shall compare the frontier orbitals of the metal carbene with those of olefin, the other reactant in eq 1b.

The metal carbene $(CH_3O)_2Mo(NH)CH_2$ has been optimized under C_s constraints with the alkylidene hydrogen atoms lying in the same plane as the spectator NH unit (**2b**). The calculated geometrical parameters for **2b**

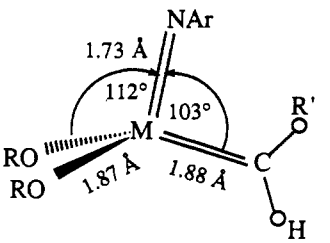

2a

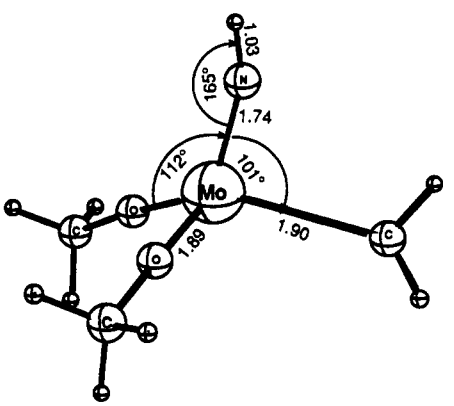

2b

agree with average M–C internuclear distances and selected bond angles for several experimentally studied carbenes[2d,e] of the type $M(CHR')(NAr)(OR)_2$ (**2a**), where M = Mo, W, Ar = 2,6-C_6H_3-*i*-Pr_2, R' = alkyl, and R = alkyl, fluoroalkyl, aryl. A structure similar to **2b**, but with the carbene coordination plane rotated 90° around the

(3) Eisenstein, O.; Hoffmann, R.; Rossi, A. R. *J. Am. Chem. Soc.* **1981**, *103*, 5582.
(4) (a) Rappe, A. K.; Upton, T. H. *Organometallics* **1984**, *3*, 1440. (b) Upton, T. H.; Rappe, A. K. *J. Am. Chem. Soc.* **1985**, *107*, 1206. (c) Rappé, A. K.; Goddard, W. A., III. *J. Am. Chem. Soc.* **1980**, *102*, 5115. (d) Rappé, A. K.; Goddard, W. A., III. *J. Am. Chem. Soc.* **1982**, *104*, 3287.
(5) Cundari, T. R.; Gordon, M. S. *Organometallics* **1992**, *11*, 55.
(6) Baerends, E. J.; Ellis, D. E.; Ros. P. *Chem. Phys.* **1973**, *2*, 41.
(7) (a) Baerends, E. J. Ph.D. Thesis, Vrije Universiteit, Amsterdam, 1975.
(8) Ravenek, W. In *Algorithms and Applications on Vector and Parallel Computers*; te Riele, H. J. J., Dekker, Th. J., van de Vorst, H. A., Eds.; Elsevier: Amsterdam, 1987.
(9) Boerrigter, P. M.; te Velde, G.; Baerends, E. J. *Int. J. Quantum Chem.* **1988**, *33*, 87.
(10) (a) Snijders, G. J.; Baerends, E. J.; Vernooijs, P. *At. Nucl. Data Tables* **1982**, *26*, 483. (b) Vernooijs, P.; Snijders, G. J.; Baerends, E. J. In Slater Type Basis Functions for the Whole Periodic System; Internal Report, Free University of Amsterdam, The Netherlands, 1981.
(11) (a) Noodleman, L.; Norman, J. G. *J. Chem. Phys.* **1979**, *70*, 4903. (b) Noodleman, L. *J. Chem. Phys.* **1981**, *74*, 5737. (c) Noodleman, L.; Baerends, E. J. *J. Am. Chem. Soc.* **1984**, *106*, 2316.
(12) Krijn, J.; Baerends, E. J. Fit Functions in the HFS-Method; Internal Report (in Dutch), Free University of Amsterdam, The Netherlands, 1984.
(13) Vosko, S. H.; Wilk, L.; Nusair, M. *Can. J. Phys.* **1990**, *58*, 1200.
(14) Becke, A. D. *Phys. Rev. A* **1988**, *38*, 2398.
(15) Perdew, J. P. *Phys. Rev. B* **1986**, *33*, 8822.
(16) (a) Ziegler, T. *J. Pure Appl. Chem.* **1991**, *63*, 873. (b) Ziegler, T.; Versluis, L. *Adv. Chem. Ser.* **1992**, *No. 230*, 75. (c) Ziegler, T.; Tschinke, T. *ACS Symp. Ser.* **1990**, *No. 428*, 277. (d) Ziegler, T.; Snijders, J. G.; Baerends, E. J. *ACS Symp. Ser.* **1989**, *No. 383*, 322. (e) Ziegler, T.; Tschinke, V.; Versluis, L. *NATO ASI Ser.* **1986**, *C176*, 189. (f) Fan, L.; Ziegler, T. *J. Am. Chem. Soc.*, in press.
(17) Ziegler, T. *Chem. Rev.* **1991**, *91*, 651.

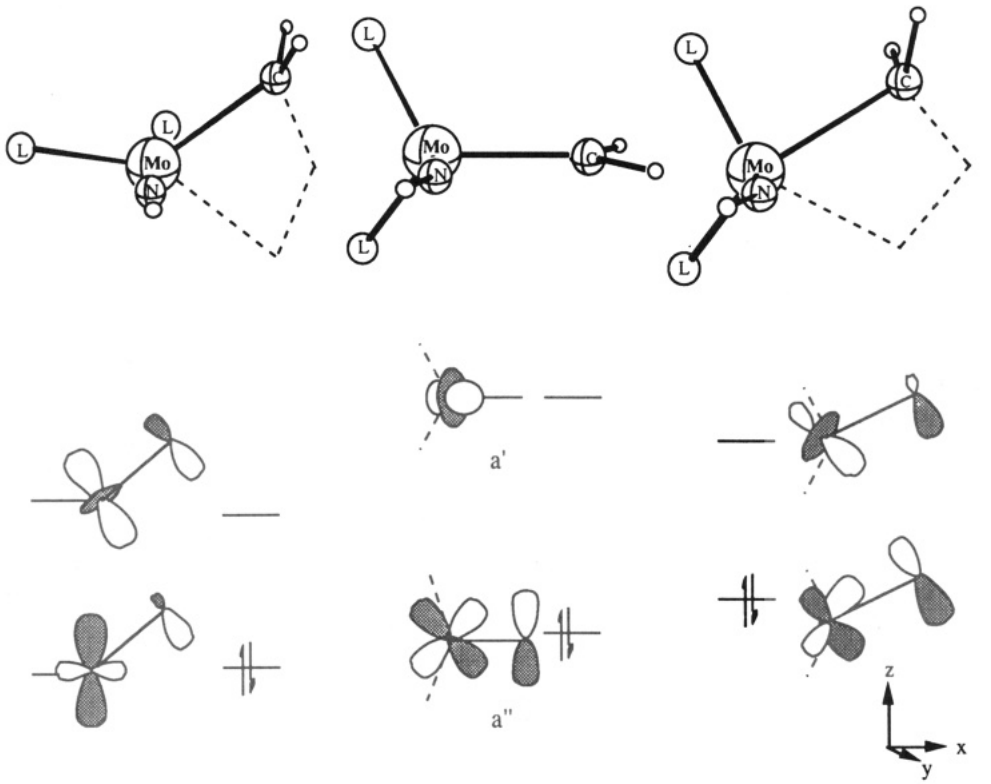

Figure 1. Correlation diagram between the frontier orbitals in the free carbene molecule (center), the carbene framework in square-pyramidal $(CH_3O)_2Mo(NH)C_3H_6$ (right side), and the carbene framework in trigonal-bipyramidal $(CH_3O)_2Mo(NH)C_3H_6$ (left side). The view is down the N–Mo bond (y axis).

Mo–C axis, was calculated to be 110 kJ mol^{-1} higher in energy. It is thus obvious that the carbene group has a clear conformational preference in the $L_2M(X)CH_2$ systems.

There are two key orbitals of importance for the reactivity of **2b** (see center of Figure 1). The carbene complex can act as a donor through the HOMO of a″ symmetry, which is composed of a d_{xz} orbital on molybdenum and a p_z orbital on carbon. The a″ HOMO is polarized toward the carbon atom and has the same nodal characteristics as the π orbital on olefin. Of higher energy is a potential acceptor orbital of a′ symmetry, mainly d_{y^2} in character. This orbital is quite different from the olefin π^*-acceptor orbital. The antibonding counterpart to the a″ HOMO would have the same nodal characteristics as the π^*-acceptor orbital on the olefin. It is, however, of too high energy to serve in this capacity and will not play any further role in our analysis.

It will also be of use to examine the frontier orbitals of the distorted carbene fragments in the TBP (**2c**) and SP conformations (**2d**) of the metallacyclobutane intermediate **1a**. Such an examination should facilitate an analysis of the bonding interaction between the olefin and carbene fragments in $L_2MoXC_3H_6$.

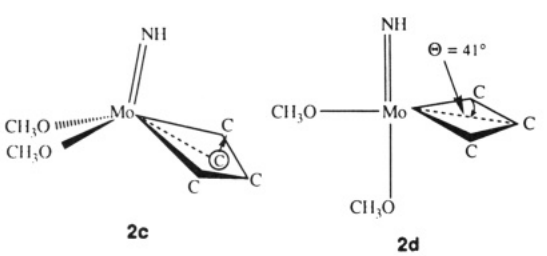

The carbene framework in the final square-pyramidal metallacycle **2c** has a geometry somewhat distorted from that of a free carbene complex, with the CH_2 ligand moved off the C_s plane in **2b** (right side of Figure 1). Through mixing between the d_{xz} and d_{yz} orbitals on molybdenum, the a″ orbital in conformation **2c** has lost the strongly bonding interaction between the metal component and the p_z/p_x combination on carbon. It is destabilized by 63 kJ mol^{-1} compared to its counterpart in **2b** (right side of Figure 1). At the same time, the d component of the a′ acceptor orbital pivots out of the C_s plane and points toward the π orbital of the adjacent olefin framework. It is achieved via an admixture with the d_{z^2} orbital on molybdenum. The resulting orbital is more stable (by 57 kJ mol^{-1}) than the a′ orbital on **2b** (Figure 1). We shall refer to this orbital as $\pi^*_{carbene}$.

On the left side in Figure 1 are displayed the corresponding donor and acceptor orbitals belonging to the carbene framework in the trigonal-bipyramidal metallacycle **2d**. The carbene framework in **2d** differs considerably from that of the free carbene $(CH_3O)_2Mo(NH)CH_2$ (**2b**). The metal center, the two oxygen atoms, and the nitrogen are seen to be coplanar in **2d**, while the carbene group is moved out of the $(CH_3O)_2Mo(NH)$ coordination plane (xy) by $\theta = 41°$. The occupied a″ orbital on the carbene framework in **2d** is composed of a $d_{z^2-x^2}$ metal hybrid rather than a d_{xz} orbital as in the case of the two other carbene structures (Figure 1). In comparison to d_{xz}, the $d_{z^2-x^2}$ metal hybrid provides better overlap with the carbene p_π carbon orbital in the case of **2d**, where $\theta = 41°$. The resulting donor orbital was calculated to be 45 kJ mol^{-1} more stable than a″ in free carbene. The metal component in the a′ acceptor orbital on the carbene fragment in **2d** is composed primarily of metal d_{z^2} and d_{xz} with an admixture of d_{yz} and

interacts in a weakly antibonding fashion with the p_z/p_x combination on carbon. The empty a′ orbital points nicely toward the π orbital of the adjacent olefin framework. The a′ acceptor orbitals in both **2c** and **2d** are quite similar in energy (Figure 1).

An analysis of the two key orbitals in Figure 1 was also performed for other $L_2Mo(NH)CH_2$ fragments with L = Cl, OCF_3. Substitution of methoxy ligands by the more electron-withdrawing chloro and trifluoroalkoxy groups gave rise to a stabilization of the two frontier orbitals. Therefore, we propose that the electron-donating methoxy groups give rise to a significant destabilization of both the donor and acceptor orbitals in Figure 1 as the electron–electron repulsion is increased around the more electron-rich metal center. In all carbene and carbene-like systems discussed, the donor and acceptor orbitals possess similar nodal characteristics. Thus, the different L groups on $L_2Mo(NH)CH_2$ affect primarily the energy of the two frontier orbitals in Figure 1.

We have also optimized a methoxycarbene structure in which the spectator NH group of **2b** has been replaced by oxygen, **2e**. We found **2b** and **2e** to have quite similar

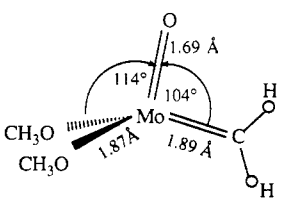

2e

structures. Further, the replacement of NH by oxygen did not appear to have any significant influence on the frontier orbitals in Figure 1. Similar dichlorocarbene and (trifluoromethoxy)carbene structures with X = O have also been optimized. The energies and compositions of the frontier orbitals were quite similar to those obtained for the corresponding systems with the NH spectator ligand.

Structure and Stability of Molybdacyclobutanes. The role of **1a** as an intermediate in Chauvin's mechanism[1] for olefin metathesis (eq 1b) has precipitated a great deal of interest in metallacyclobutanes. Studies[1] on olefin metathesis processes mediated by Schrock's catalyst $L_2Mo(X)CH_2$ have revealed intermediate metallacycles with trigonal-bipyramidal (**1a**) as well as square-pyramidal (**1c**) conformations. The relation between the electronegativity of L and the structure and stability of $L_2Mo(X)C_3H_6$ is of considerable experimental interest, and a spectrum of ligands with different electronegativities and considerable bulk has been investigated. Experimental studies[1] have focused on the structure and reactivity of metallacyclobutanes of the type $(RO)_2M(X)C_3H_4R'R''$, where M = Mo, W, Ta, R = alkyl, fluoroalkyl, aryl, R′, R″ = H, alkyl, substituted alkyl, and X = NAr.

In our calculations we have studied the equilibrium geometries and corresponding relative energies of the molybdacyclobutanes $L_2Mo(X)C_3H_6$ in conformations **1b** and **1c** as well as their stability toward decomposition into metal carbene $L_2Mo(X)CH_2$ and free olefin. The impact of the coligand L has been probed by introducing the groups L = Cl, OCH_3, OCF_3, having different electronegativities. The spectator NAr ligand has been replaced by the isoelectronic NH group. We have also carried out a complete set of calculations on $L_2Mo(O)C_3H_6$, where the NAr ligand is replaced by oxygen. This series should enable us to establish how critical small changes in the electronic structure of the spectator ligand are for the structure and stability of molybdacyclobutane.

With $(CH_3O)_2Mo(NH)C_3H_6$ as an example, we will discuss the structural differences between the two types of metallacycles. The square-pyramidal metallacyclobutane **4** is characterized by a rather small C_α–Mo–C_α angle of 62.7° and a C_α–C_β–C_α angle of only 97°. The remaining lateral angles of 96.7° complete the definition of the ring system. The corresponding bond angles in the

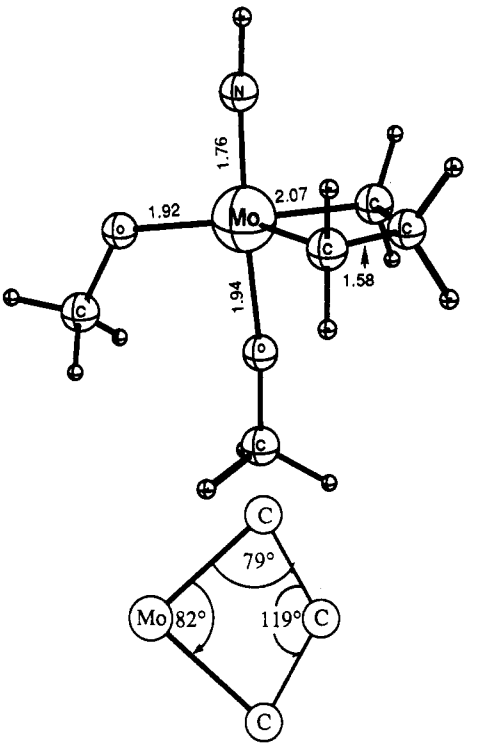

3

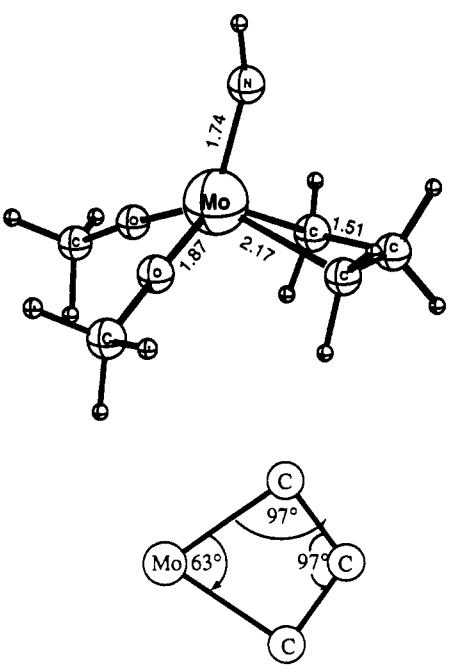

4

trigonal-bipyramidal structure **3** were calculated to be 82, 119.2, and 79.4°, respectively. In the square-pyramidal intermediate, the Mo–C_α bond distance of 2.17 Å is 0.10

Table I. Optimized Structures[a] for $L_2Mo(X)C_3H_6$ in the TBP Conformation 1b

	$L_2Mo(X)C_3H_6$					
	L = Cl, X = O	L = Cl, X = NH	L = CH_3O, X = O	L = CH_3O, X = NH	L = CF_3O, X = O	L = CF_3O, X = NH
Mo=X	1.70	1.74	1.72	1.76	1.70	1.75
Mo—C_α	2.05	2.06	2.07	2.07	2.07	2.06
Mo—C_β	2.31	2.34	2.35	2.36	2.34	2.33
C_α—C_β	1.58	1.58	1.57	1.58	1.58	1.57
C_α–Mo–C_α	84.0	83.3	82.2	82.0	82.5	82.9
C_α–C_β–C_α	120.7	119.6	119.9	119.2	120.1	119.9
Mo–C_α–C_β	77.5	78.5	78.9	79.4	78.6	78.6
X–Mo–C_β	87.1	93.8	89.2	91.9	84.7	89.5
X–Mo–C_α	87.1	92.0	89.3	91.3	87.3	90.0
X–Mo–L_{ax}	192.4	186.6	184.1	185.1	192.2	187.0
X–Mo–L_{eq}	102.2	98.7	94.0	96.7	96.6	97.9
L_{ax}–Mo–L_{eq}	90.2	87.9	90.1	88.5	95.6	89.1
L_{ax}–Mo–C_α	83.7	82.1	87.7	84.8	83.5	84.8
L_{eq}–Mo–C_α	137.1	137.1	138.8	138.3	138.7	137.9
MoC_3 (torsion)	0.0	3.4	0.7	0.4	5.3	2.5

[a] Bond distances are in angstroms; angles are in degrees.

Table II. Optimized Structures[a] for $L_2Mo(X)C_3H_6$ in the SP Conformation 1c

	$L_2Mo(X)C_3H_6$					
	L = CL, X = O	L = Cl, X = NH	L = CH_3O, X = O	L = CH_3O, X = NH	L = CF_3O, X = O	L = CF_3O, X = NH
Mo=X	1.68	1.72	1.70	1.74	1.67	1.71
Mo—C_α	2.18	2.20	2.18	2.17	2.18	2.17
Mo—C_β	2.79	2.88	2.83	2.79	2.82	2.81
C_α—C_β	1.51	1.51	1.52	1.51	1.50	1.50
C_α–Mo–C_α	62.0	62.4	63.2	62.7	61.2	61.5
C_α–C_β–C_α	96.0	98.1	98.0	97.0	95.3	95.6
Mo–C_α–C_β	101.0	99.8	118.7	96.7	98.2	97.8
X–Mo–C_α	100.0	99.3	100.7	100.4	97.0	96.6
L–Mo–L	109.4	101.5	101.1	99.4	111.7	113.7
L–Mo–C_α	82.3	83.5	86.4	84.4	80.9	89.9
X–Mo–L	113.2	117.5	113.1	117.2	115.1	112.6
MoC_3 (torsion)	0.0	0.1	12.3	26.3	26.9	27.0

[a] Bond distances are in angstroms; angles are in degrees.

Å longer than that of trigonal-bipyramidal structure. On the other hand, the C_α–C_β bond distances in **4** are 0.07 Å shorter than those in **3**. The above parameters lead to a significantly larger Mo–C_β separation of 2.79 Å in **4** and an elongated-kite shape of the metallacycle core geometry compared to the one found in the trigonal-bipyramidal structure. The corresponding Mo–C_β distance in **3** was calculated to be 2.36 Å. The two equivalent Mo–O bond distances of 1.87 Å in the SP structure **4** are somewhat shorter than the Mo–O_{eq} bond length in **3** at 1.92 Å. The axial Mo–O distance in the TBP structure **3** with R(Mo–O_{ax}) = 1.94 Å is seen to be even longer due to the trans effect of the NH ligand. Also, there is a difference between the O–Mo–O bond angles in the two conformations. Thus, the O–Mo–O angle in the SP structure **4** at 99.4° is wider than the O–Mo–O angle of 88.5° in the TBP conformation **3**.

The trends noted for the $(CH_3O)_2Mo(NH)C_3H_6$ system are also present in the optimized structures for $L_2Mo(NH)C_3H_6$ with L = Cl and OCF_3 as well as for the corresponding complexes involving oxygen as a spectator ligand. In all cases, the square-pyramidal structures were characterized by longer molybdenum–carbon bond distances as well as a longer Mo–C_β separation across the ring. In general, the C_α–Mo–C_α and C_α–C_β–C_α angles were found to be about 20° wider in the SP structures (**4**) than in the TBP geometries (**3**). Also, the L–Mo–L angle was calculated to be wider (~105°) in the SP geometry than in the TBP conformation (~90°), and an elongation of the axial Mo–L bond was noticeable in the TBP structures. The structural data for the TBP and SP intermediates are presented in Tables I and II, respectively.

The calculated parameters for the ring core in the two conformations **3** and **4** compare well with the available structural data for the olefin metathesis intermediates.[2] Several square-pyramidal tungstacycles and a molybdacycle have been isolated and structurally characterized, and the following parameters were reported: relatively long M–C_β distances of about 2.77–2.79 Å and approximately single M–C_α bonds of about 2.14 Å as well as small C_α–M–C_α and C_α–C_β–C_α angles of about 63–65 and 93–104°, respectively. Similarly, both the theoretical internuclear distances and the bond angles in the trigonal-bipyramidal structures are in close agreement with the published experimental data,[2c,f] where a typical W–C_β distance is 2.3–2.4 Å, the M–C_α bond length is 2.04–2.10 Å, and the C_α–M–C_α and C_α–C_β–C_α angles are about 82–84 and 116–121°, respectively. All experimental trigonal-bipyramidal intermediates were reported to have planar ring cores, while the square-pyramidal structures possessed some torsion of the MC_3 ring (10–34°). We have calculated up to 27° torsion of the ring cores in the optimized geometries for **3** and **4** as well as the structures for the corresponding cyclic species $L_2Mo(X)C_3H_6$ involving L = Cl, OCF_3 and X = O, NH.

The structural characteristics of the SP and TBP conformations can be rationalized by analyzing the interaction between L_2MoX and the C_3H_6 moieties in the two types of metallacycles. These interactions involve primarily a pair of singly occupied frontier orbitals of a′

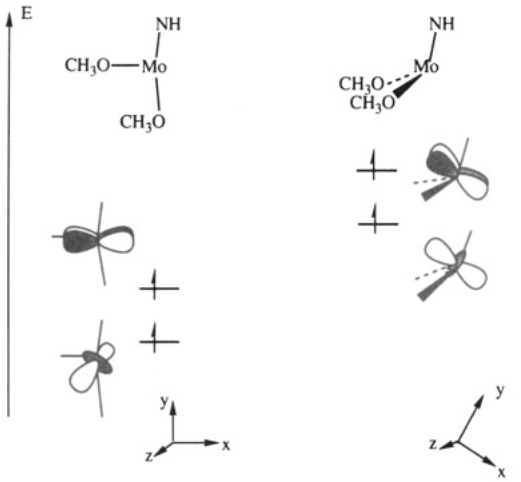

Figure 2. d component of the highest lying singly occupied orbitals on $(CH_3O)_2Mo(NH)$ metal fragments in **3** (left side) and **4** (right side).

and a″ symmetry on each of the L_2MoX and C_3H_6 fragments. The interactions between the four singly occupied orbitals are responsible for the formation of two Mo–C_α σ bonds.

The two singly occupied frontier orbitals on the C_3H_6 fragment of a′ and a″ symmetry are shown as **5a** and **5b**, respectively. In the intermediates **3** and **4**, the nodal

5a **5b**

characteristics of the frontier orbitals stay virtually the same. As mentioned above, the C–C–C angle in the C_3H_6 fragment for the trigonal-bipyramidal structure was calculated to be 119°, while the corresponding angle in the square-pyramidal conformation was found to be 97°. The two singly occupied frontier orbitals on the $(CH_3O)_2$-Mo(NH) metal fragments are given in Figure 2. In the metal fragment belonging to the intermediate **3**, a′ is described best as a d_{z^2} orbital (see the left side of Figure 2). In the metal fragment for the square-pyramidal intermediate, the largest amplitude of a′ comes from the d_{x^2} orbital on molybdenum. The singly occupied orbitals of a″ symmetry are mainly d_{xz} in character for both metal fragments.

The interactions between fragment orbitals of a′ and a″ symmetries are shown in **5c** and **5d**, respectively, for the TBP structure **3**. It is clear from **5c** and **5d** that the

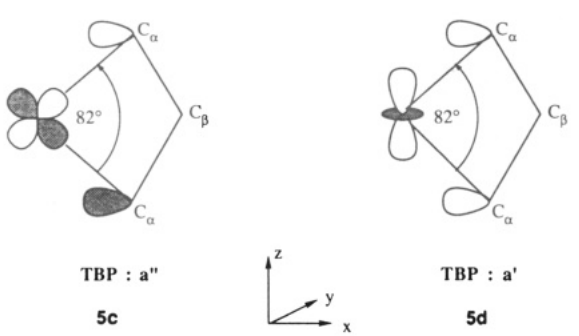

5c **5d**

calculated C_α–Mo–C_α bond angle of 82° is a compromise between a more acute angle which would optimize the overlaps in **5c** and a wider angle which would be optimal for the interactions in **5c**. The optimized Mo–C_α and C_α–C_β distances along with the C_α–Mo–C_α bond angle of 82° determines completely the structure of the kite-shaped Mo–C_3 core with the relatively short Mo–C_β distance of 2.36 Å. The corresponding interactions between fragment orbitals of a′ and a″ symmetries are shown in **5e** and **5f**, respectively, for the SP structure **4**. The optimal C_α–

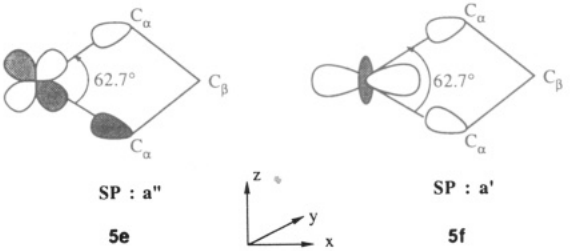

5e **5f**

Mo–C_α angle for the interaction in the a″ representation **5e** is quite similar to that found for the same symmetry in the TBP conformation **5c**. On the other hand, the a′ representation **5f** with the metal component along the *x* axis calls for quite an acute C_α–Mo–C_α bond angle as opposed to a wider angle in the TBP case **5d**, where the metal component is situated along the *z* axis. The difference between the orientations of the metal component in the two a′ interactions is responsible for the C_α–Mo–C_α angle being smaller in the SP conformation **4** than in the TBP conformation **3**. We optimize the C_α–Mo–C_α angle in **4** at 62.7°.

A C_α–Mo–C_α angle of 62.7° for the kite-shaped Mo–C_3 core in the SP structure would give rise to a C_α–C_β–C_α angle of 86° and a Mo–C_β bond length of 2.91 Å if the same Mo–C_α (2.07 Å) and C_α–C_β (1.58 Å) distances were adopted as in the TBP geometry **5g**. The acute angle of 86° would

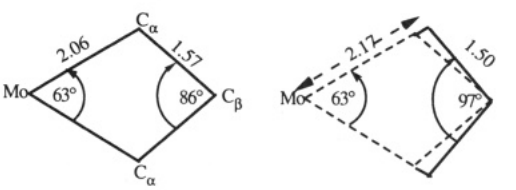

5g **5h**

put too much strain on the C_3H_6 fragment. The strain can be relieved by increasing the Mo–C_α distance and, in the process, shortening the C_α–C_β bond (**5h**). We find in our calculations that the Mo–C_α distance is elongated to 2.17 Å, which gives rise to a C_α–C_β distance of 1.50 Å and a C_α–C_β–C_α angle of 97°.

We have provided a rationale for the different structural characteristics of the SP and TBP conformations based on the orbital interactions in **5c–f**. A possible explanation was given for the fact the C_α–Mo–C_α angle is smaller in SP than in TBP. It has further been shown why the Mo–C_α and Mo–C_β distances are larger, and the C_α–C_β bond shorter, in SP compared to TBP. Our rationalization for the shorter Mo–C_β distance in the TBP structure did not invoke any Mo–C_β bonding interaction. In fact, we did not find any from our analysis of the molecular orbitals. Also, we have not implied a weaker Mo–C_α interaction in our explanation for the longer Mo–C_α bond in the SP structure. On the contrary, we shall shortly show that the Mo–C_α interaction in some cases might be stronger in SP than in TBP.

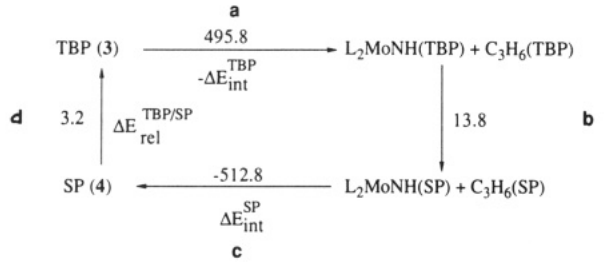

Figure 3. Haber cycle analyzing the relative stabilities of **4** and **3** (L = OCH_3). Energies are in kJ mol^{-1}.

The relative stability of the SP (**4**) and TBP (**3**) structures, $\Delta E_{rel}^{TBP/SP} = E(SP) - E(TBP)$, can be analyzed by considering the Haber cycle of Figure 3 in which **3** is converted into **4**, in the four steps **a**–**d**.

Step **a** dissociates $(CH_3O)_2Mo(NH)C_3H_6$ of the TBP conformation **3** into the C_3H_6 and $(CH_3O)_2Mo(NH)$ moieties without changing the structure of the two fragments, C_3H_6 (TBP) and $(CH_3O)_2Mo(NH)$ (TBP). The total dissociation energy for this process is given by $-\Delta E_{int}^{TBP}$ = 495.8 kJ mol^{-1} (Figure 3), where ΔE_{int}^{TBP} is the interaction energy between C_3H_6 (TBP) and $(CH_3O)_2$-Mo(NH) (TBP) in **3**. This value translates into a bond-snapping energy of 248 kJ mol^{-1} (59.3 kcal mol^{-1}) for each Mo–C_α bond, which is somewhat larger than for an ordinary metal–alkyl bond (~50 kcal mol^{-1}).

The next step, **b**, transforms (deforms) the two fragments from their TBP conformations into the structures they will take up in **4**, C_3H_6 (SP) and $(CH_3O)_2Mo(NH)$ (SP). In our study, we found that the C_3H_6 (TBP) fragment is 15.3 kJ mol^{-1} more stable than C_3H_6 (SP). This can be explained by observing that the C_α–C_β–C_α angle of 119° in C_3H_6(TBP) is somewhat closer to the ideal 109.5° angle than the corresponding angle of 97° in C_3H_6 (SP). On the other hand, the metal fragment $(CH_3O)_2Mo(NH)$ (SP) was calculated to be 6.4 kJ mol^{-1} more stable than $(CH_3O)_2Mo(NH)$ (TBP). The most obvious reason[2c] for this difference is that in $(CH_3O)_2Mo(NH)$ (TBP) both the axial alkoxy ligand and the spectator NH group compete as π donors for the same empty orbital on molybdenum (**6**). The weakened bonding interaction between molybdenum and nitrogen can be seen in a longer Mo–N distance in $(CH_3O)_2Mo(NH)$ (TBP; **3**) compared to that in $(CH_3O)_2Mo(NH)$ (SP; **4**). By the same token, the axial Mo–O_{ax} bond length in **3** is much longer (by 0.19 Å) than the equatorial Mo–O_{eq} bond length. The unfavorable interaction in **6** contributes through the longer bonds to the higher energy of $(CH_3O)_2Mo(NH)$ (TBP) compared to $(CH_3O)_2Mo(NH)$ (SP). The total deformation energy in step **b** is stabilizing (negative) and amounts to −8.9 kJ mol^{-1}. The third step, **c**, combines the $(CH_3O)_2Mo(NH)$ (SP) and C_3H_6 (SP) fragments into $(CH_3O)_2Mo(NH)C_3H_6$ of SP geometry (**4**). The energy gained from this process is ΔE_{int}^{SP} = 512.8 kJ mol^{-1} (Figure 3). Thus, the SP M–C_α bonds (256 kJ mol^{-1}) are slightly stronger than their TBP counterparts, in spite of the fact that the former are longer. We attribute this to slightly better total overlaps in **5e,f** compared to those in **5c,d**.

6

Table III. Calculated Relative Energies[a] of Square-Pyramidal (SP) and Trigonal-Bipyramidal (TBP) $L_2Mo(NH)C_3H_6$ (L = Cl, OCH_3, OCF_3)

L	$\Delta E[L_2Mo(NH)]^b$	$\Delta E[C_3H_6]^c$	$E_{int}^{SP} - E_{int}^{TBP}$ [d]	$\Delta E_{rel}^{TBP/SP}$ [e]
Cl	−42.8	19.1	17.9	5.8
OCH_3	−6.4	20.2	−17.0	3.2
OCF_3	−17.4	20.6	22.1	−25.3

[a] All energies in kJ mol^{-1}. [b] $\Delta E[L_2Mo(NH)]$ = (energy of $L_2Mo(NH)$ in SP conformation) − (energy of $L_2Mo(NH)$ in TBP conformation). [c] $\Delta E[C_3H_6]$ = (energy of C_3H_6 in SP conformation) − (energy of C_3H_6 in TBP conformation). [d] ΔE_{int}^{SP} and ΔE_{int}^{TBP} are defined in Figure 3. [e] $\Delta E_{rel}^{TBP/SP} = \Delta E^{TBP} - \Delta E^{SP}$ is the energy difference between the TBP and SP conformations of $L_2Mo(NH)C_3H_6$. We have $\Delta E_{rel}^{TBP/SP} = -\{\Delta E[L_2Mo(NH)] + \Delta E[C_3H_6] + [\Delta E_{int}^{SP} - \Delta E_{int}^{TBP}]\}$.

The last step, **d**, transforms SP into TBP. The required energy is $\Delta E_{rel}^{TBP/SP}$ = 8.1 kJ mol^{-1} (Figure 3), which means that the SP geometry **4** is more stable than the TBP conformation **3** by the same amount. Our analysis indicates that the major factors in favor of SP compared to TBP are a more stable metal fragment, $(CH_3O)_2Mo(NH)$ (SP), and a stronger interaction between the $(CH_3O)_2$-Mo(NH) (SP) and C_3H_6 (SP) frameworks. On the other hand, the relative stability of the two C_3H_6 units favors the TBP geometry **3**.

Experimental work on the structure and reactivity of W(VI) and Mo(VI) metallacyclobutanes[2] finds evidence for the presence of TBP as well as SP structures in solution. In fact, the two conformations are often observed to coexist in equilibrium. Feldman[2c] et al. have demonstrated that the equilibrium is shifted toward TBP for electron-withdrawing alkoxides such as $OC(CF_3)_2(CF_2CF_2CF_3)$, whereas the electron-donating alkoxide O-*t*-Bu favors SP. The balance is very fine indeed, with $OC(CH_3)_2CF_3$ affording mostly SP and $OC(CF_3)_2CH_3$ primarily TBP.

In Table III, we present the relative stabilities, $\Delta E_{rel}^{TBP/SP}$, of the SP and TBP conformations for $L_2Mo(NH)C_3H_6$ with L = OCH_3 as well as L = Cl, OCF_3. We find in agreement with experiment that the SP conformation is lowest in energy for the electron-releasing alkoxide group L = OCH_3, whereas the electron-withdrawing alkoxide L = OCF_3 prefers the TBP structure. The analogous $L_2Mo(O)C_3H_6$ systems have not been studied experimentally. We find that L = OCH_3 as well as L = Cl, OCF_3 prefer a SP conformation (Table IV). It follows from the decomposition in Tables III and IV that the $L_2Mo(X)$ metal fragment invariably prefers the SP conformation, whereas the C_3H_6 moiety favors the TBP structure. The only pivotal term in the decomposition of Figure 3 is $E_{int}^{SP} - E_{int}^{TBP}$. It is negative for $(OCH_3)_2$-$Mo(NH)C_3H_6$ (Table III) as well as for all three L_2Mo-$(O)C_3H_6$ systems (Table IV). Thus, in those cases the interaction between $LMo(X)CH_2$ and C_3H_6 is stronger for the SP structure. The opposite is found to be the case for $(OCF_3)_2Mo(NH)C_3H_6$ and $Cl_2Mo(NH)C_3H_6$, where $E_{int}^{SP} - E_{int}^{TBP}$ is positive (Table III). Unfortunately, it was impossible to find any single orbital interaction responsible for the change in sign of $E_{int}^{SP} - E_{int}^{TBP}$. However, we

Table IV. Calculated Relative Energies[a] of Square-Pyramidal (SP) and Trigonal-Bipyramidal (TBP) $L_2Mo(O)C_3H_6$ (L = Cl, OCH_3, OCF_3)

L	$\Delta E[L_2Mo(O)]^b$	$\Delta E[C_3H_6]^c$	$\Delta E_{int}^{SP} - \Delta E_{int}^{TBP}$ [d]	$\Delta E_{rel}^{TBP/SP}$ [e]
Cl	−57.7	27.8	−3.0	32.9
OCH_3	−21.8	14.6	−14.5	21.7
OCF_3	−35.4	23.0	−5.0	17.4

[a] All energies in kJ mol^{-1}. [b] $\Delta E[L_2Mo(O)]$ = (energy of $L_2Mo(O)$ in SP conformation) − (energy of $L_2Mo(O)$ in TBP conformation). [c] $\Delta E[C_3H_6]$ = (energy of C_3H_6 in SP conformation) − (energy of C_3H_6 in TBP conformation). [d] ΔE_{int}^{SP} and ΔE_{int}^{TBP} are defined in Figure 3. [e] $\Delta E_{rel}^{TBP/SP} = \Delta E^{TBP} - \Delta E^{SP}$ is the energy difference between the TBP and SP conformations of $L_2Mo(O)C_3H_6$. We have $\Delta E_{rel}^{TBP/SP} = -\{\Delta E[L_2Mo(O)] + \Delta E[C_3H_6] + [\Delta E_{int}^{SP} - \Delta E_{int}^{TBP}]\}$.

shall later give an alternative analysis of the factors behind the balance between SP and TBP conformations.

Formation and Decomposition of Metallacycles. We have carried out a detailed analysis of the process in eq 1b, where the metal carbene of the type **2b** reacts with ethylene to form the metallacycle **4** with a SP conformation as well as **3** in a TBP arrangement. In our analysis below, we have used Cl to model real-life alkoxy substituents. For one reason, chlorine lies between methoxy and trifluoromethoxy ligands on the electrodonicity scale.[18] For another, it was computationally more economical to carry out such detailed calculations using ligands with a smaller electron count. We shall refer to the chloro-substituted metallacycles of SP and TBP geometries as **4a** and **3a**, respectively.

We shall first discuss the formations of the metallacycle **4** with a SP conformation. For this process, ethylene is allowed to approach the metal carbene by gradually decreasing the $R(Mo–C_1)$ distance (**7a**) between the

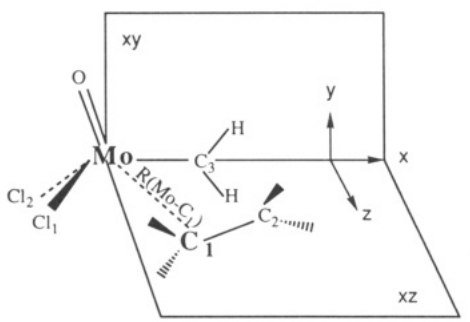

7a

molybdenum center and one of the olefin carbons. The reaction coordinate $R(Mo–C_1)$ was varied from 4.5 Å, where ethylene and the metal carbene are virtually noninteracting, to 2.18 Å, which is the $R(Mo–C_1)$ distance in the final metallacycle **4a** of SP geometry. The variation of $R(Mo–C_1)$ was carried out in six steps, and for each of these steps all other degrees of freedom were optimized. The energy of the reacting system is plotted in Figure 4a as a function of the reaction coordinate $R(Mo–C_1)$.

It follows from our analysis that the olefin approaches **2b** perpendicular to the O–Mo–C_3 (xy) plane of the metal carbene (**7a**) in such a way that the $C_1–C_2$ olefin and Mo–C_3 carbene bonds are coplanar (xz of **7a**). The position of the $C_1–C_2$ olefin and Mo–C_3 carbene bonds are shown in **7b** for different values of the reaction coordinate $R(Mo–C_1)$ in **8**, **9**, **10a**, and **4a**. The position of Cl_1, Cl_2, and the

(18) Vollhardt, K. P. C. In *Organic Chemistry*; H. F. Freeman: New York, 1987; p 900.

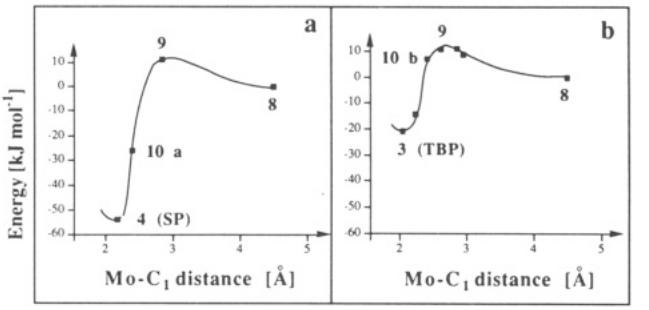

Figure 4. Reaction profiles for the dissociation of the $Cl_2Mo(O)C_3H_6$ metallacycles: (a) square pyramidal; (b) trigonal bipyramidal.

spectator oxygen hardly changes during the reaction. The minor adjustments of the $Cl_2Mo(O)$ framework are not indicated in **7b**. The energy for each of the en route structures **8**, **9**, and **10a** are given in Figure 4a, where we present a reaction energy profile for the process.

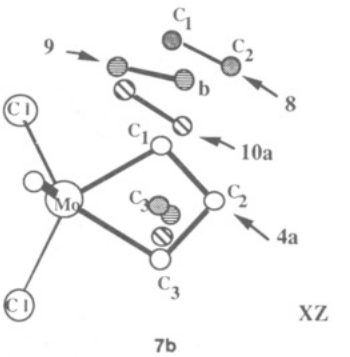

7b

There is virtually no interaction between ethylene and the metal carbene at the early stages (**8**) of the reaction where $R(Mo–C_1) > 4$ Å, and both reacting fragments are undistorted from the free state. The energy is rising steadily from **8** ($R(Mo–C_1) = 4.5$ Å) to **9** ($R(Mo–C_1) = 2.89$ Å) by a total of 11.2 kJ mol^{-1}. The structure **9** can be considered as a transition state for the process in eq 1b since it is situated at the highest energy point on the approximate reaction profile (Figure 4a). However, no attempt was made to verify whether **9** has a single normal mode with an imaginary frequency. The transition-state structure **9** is basically an olefin π complex with an approximately trigonal-bipyramidal geometry. In this trigonal structure one of the chlorine ligands and the median of the olefin C–C bond are taking up the axial positions, whereas the spectator oxygen, another chlorine ligand, and the carbene carbon atom are lying in the equatorial plane of a bipyramid. The C=C bond distance in the weakly coordinated olefin was calculated to be 1.35 Å (versus 1.33 Å in a free molecule). At the same time, the hydrogen atoms in the olefin have started to bend away from the target carbene complex and the Mo–C carbene bond distance has increased from 1.88 to 1.90 Å as the carbene group moves out of the xy plane (**7a**).

The formation of the π-complex is followed by a steep decrease in the total energy until the product **4a** is formed. All three carbon atoms undergo an $sp^2 \rightarrow sp^3$ rehybridization and eventually become involved in the MC_3 core. It is interesting to note that the $sp^2 \rightarrow sp^3$ rehybridization takes place at the very last stages of the reaction. Thus, **10a** has essentially retained its olefin and carbene double bonds as well as the sp^2 hybridization around the carbon centers although it has a $R(Mo–C_1)$ distance of 2.40 Å,

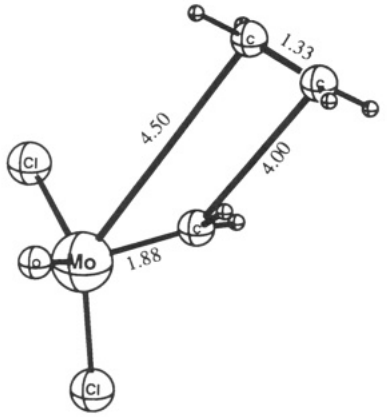

8

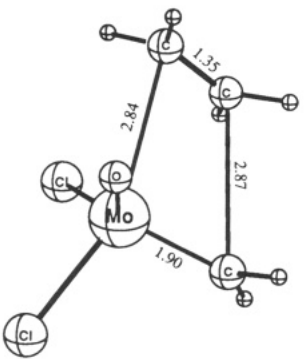

9

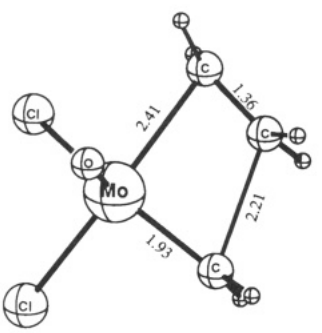

10a

which is only ~0.2 Å shorter than the final Mo–C_1 bond length in **4a**. Also, the C_2–C_3 distance at 2.18 Å (**10a**) is much longer than the final C_2–C_3 single-bond distance of 1.51 Å in **4a**. Thus, the C–C bond formation is seen to lag behind the Mo–C bond formation.

Structure **10a** represents a nucleophilic attack of the olefin C_1 carbon (**7b**) at the metal center. This attack precedes the nucleophilic attack of the carbene C_3 center at the olefinic C_2 carbon, which takes place at the final stages of the reaction with $R(C_1$–Mo) between 2.40 and 2.18 Å. The nucleophilic attack of the olefin C_1 carbon on the metal center involves the ethylene π donor orbital and the a′ metal carbene acceptor orbital (**11a**). The attack

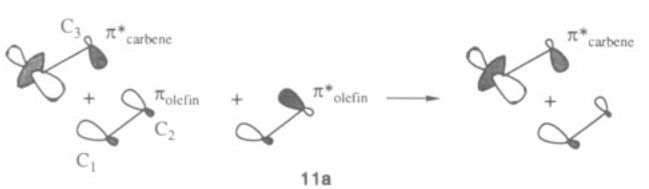

11a

is enhanced by an admixture of π^* on olefin which polarizes the donor orbital toward the approaching C_1 carbon. The subsequent attack by the metal involves donation of charge from the π carbene donor orbital to π^* on olefin which is now polarized toward C_2 (**11b**). This donation induces a

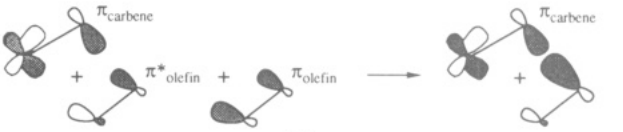

11b

reduction in the C=C and Mo=C bond orders to 1 as well as the desired $sp^2 \rightarrow sp^3$ rehybridization. The gain in energy from the $\pi_{carbene}$ to π^*_{olefin} donation is largely canceled by the energy required (324.8 kJ mol^{-1}) for the $sp^2 \rightarrow sp^3$ rehybridization. We have seen that the formation of metallacyclobutane in the SP conformation involves transfer of charge to π^*-type orbitals from π-donor orbitals (**11a** and **11b**). This transfer is facilitated by the fact that overlaps between π^* and π orbitals are maintained throughout the reaction (**11c** and **11d**). It is also clear from **11c** and **11d** that a concerted approach in which both donor/acceptor interactions **11c** and **11d** are turned on at the same time would lead to C_2–C_3 and M–C_1 antibonding interactions, respectively.

11c **11d**

Feldman et al.[2c] have described the reaction in eq 1 by a sequence of steps quite similar to those given in Figure 4. However, their description was given in a somewhat different language with a strong bearing on organic nomenclature. We shall, for the sake of compatibility, reconcile their description of the process with our account. Feldman et al. viewed the initial stages of the reaction leading to **8** (path **a** of Figure 5) as an attack of ethylene on the C–L_1–O face of the $L_2Mo(X)CH_2$ carbene. This attack results in the SP olefin complex **9**. The evolution of the π complex into the SP intermediate **4a** is seen to occur via a Berry-type pseudorotation. According to path **a**, the spectator oxygen atom, originally in the equatorial plane of the trigonal bipyramid **9**, adopts an apical position in the en route square pyramid **10a**. Further transformation leads to the square-pyramidal intermediate structure **4a**.

We have now completed our discussion of path a in Figure 5, which leads to the formation of the SP metallacycle **4a**. We shall next turn to a discussion of the alternative process leading to the TBP metallacycle **3a**. This process is indicated in Figure 5 as route **b**. We shall in our study of **b** make use of the same $Cl_2Mo(O)C_3H_6$ model system employed for the discussion of **a**. The profile for **b** was traced by starting with $Cl_2Mo(O)C_3H_6$ of the TBP conformation **3a** and gradually increasing the Mo–C_1 distance from 2.07 Å in the metallacycle **3a** to 5 Å for complete separation of ethylene and the metal carbene Cl_2MoCH_2. The change in the Mo–C_1 distance from 2.07 to 5 Å was carried out in six steps, and in each step all other degrees of freedom were fully optimized. Thus, use has been made of the same Mo–C_1 distance as reaction coordinate for both **a** and **b**. The reaction profile corresponding to path **b** is given in Figure 5b.

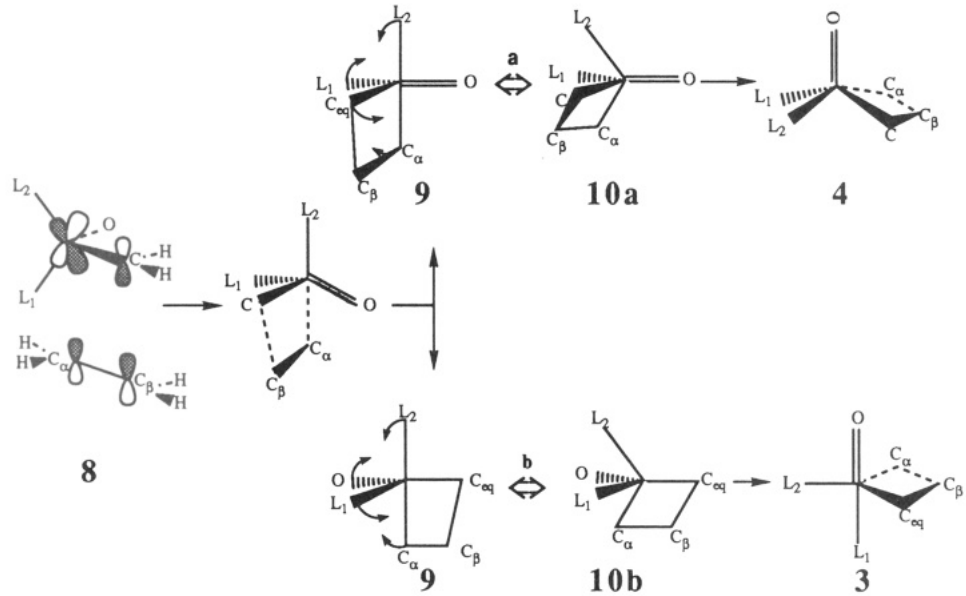

Figure 5. The two possible Berry pseudorotation routes leading to SP and TBP metallacyclobutanes.

The general geometrical transformation along path **b** is quite simple. Ethylene approaches the metal carbene in the xz plane of **7a** in a way completely analogous to the course taken in path **a**. The only difference between a and **b** is that the $Cl_2Mo(O)$ framework hardly changes geometry in **a**, whereas the $Cl_2Mo(O)$ moiety in **b** undergoes a drastic deformation as ethylene approaches the carbene molecule. The transformation of the $Cl_2Mo(O)$ fragment in **b** involves a movement of the spectator oxygen in the xy plane of **7a** to a position along the y direction. At the same time the two chlorines move into the xy plane of **7a** in such a way that Cl_1 ends up trans to oxygen and Cl_2 along the $-x$ direction. We shall now give a more detailed description of path **b** in connection with the profile given in Figure 4b.

Following path **b** from **9** at $R(Mo–C_1)$ = 2.84 Å to **10b** at $R(Mo–C_1)$ = 2.41 Å leads to an elongation of the olefinic double bond by 0.16 Å and an increase in the Mo–C_3 bond length by 0.13 Å. The three carbon centers have in addition

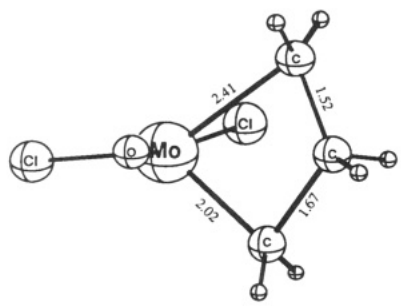

10b

undergone an sp^2 to sp^3 rehybridization, and the $Cl_2Mo(O)$ fragment has nearly completed the geometrical rearrangement discussed above. The cost in energy of the many deformations is compensated for by the formation of a Mo–C_1 bond as well as a C_2–C_3 carbon bond (**10b**). In total the energy has gone down by ~4 kJ mol^{-1} in passing from **9** at $R(Mo–C_1)$ = 2.84 Å to **10b** at $R(Mo–C_1)$ = 2.41 Å. After **10b** path b proceeds smoothly to **3a** at $R(Mo–C_1)$ = 2.07 Å with a total drop in energy of 26 kJ mol^{-1} (Figure 4b).

There is an important difference between paths **a** and **b**. It concerns the timing of the C_2–C_3 carbon bond formation as well as the rehybridization around the carbon centers. In path **a** at $R(Mo–C_1)$ = 2.41 Å (**4a**) the C_2–C_3 distance is 2.21 Å with little C–C bond formation and a modest stretch of either the Mo–C_3 carbene distance or the C_1–C_2 olefin bond. Consequently, little rehybridization has taken place around the carbon centers. In contrast, at the same value of 2.41 Å (**10b**) for the Mo–C_1 reaction coordinate in path **b** an almost full C_2–C_3 carbon bond has formed. In addition, both the Mo–C_3 carbene distance and the C_1–C_2 olefin bond have stretched considerably and the carbon centers have changed to an sp^3 hybridization.

We have previously studied the shape of the donor/acceptor orbitals **11c** and **11d** on the metal–carbene fragment of **10a** in path **a** at $R(Mo–C_1)$ = 2.40 Å and concluded that their shape necessitated a two-step attack with Mo–C_1 bond formation preceding C_2–C_3 bond formation. The corresponding donor/acceptor orbitals for the metal–carbene fragment of **10b** in path b at $R(Mo–C_1)$ = 2.41 Å are given in **12a** and **12b**, respectively. The

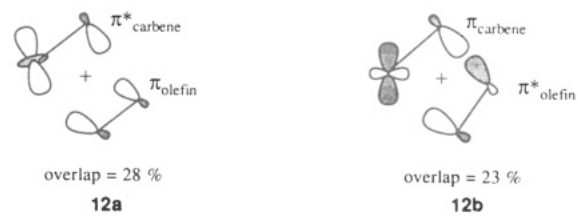

hybridizations around the metal center in the two sets of orbitals are quite different, as the result of different Cl_2MoO coordination geometries (see Figure 1 and previous discussion). Further, the donor/acceptor set in **12a** and **12b** are seen to be more prone to concerted Mo–C_1 and C_2–C_3 bond formation. This is clear in **12a**, where bonding overlaps can develop along the Mo–C_1 bond and the C_2–C_3 axis. In **12b** the overlap is bonding along the C_2–C_3 vector and nearly zero at the Mo–C_1 terminal. The zero overlap at the Mo–C_1 part arises from the special nodal structure and small amplitude of the metal hybrid.

Our investigation of the reaction between the olefin and the $L_2Mo(O)CH_2$ carbene has been restricted to the case where L = Cl. We have not traced the reaction profiles for the other carbene systems with L = OCH_3 and OCF_3.

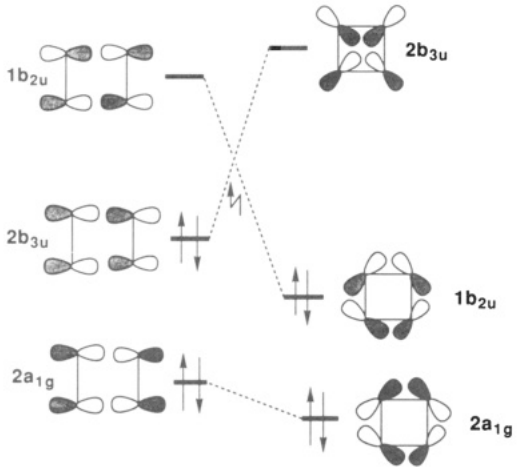

Figure 6. Correlation diagram for the formation of cyclobutane from two ethylene molecules (orbital labeling in D_{2h} symmetry).

Neither have we discussed the case where the spectator oxygen was replaced by NH. We expect in all cases that the reaction between olefin and the metal carbene will proceed with a modest barrier. Exactly which factors will favor one of the two conformations **1b** and **1c** for the metallacycle will be discussed later. It is further important to point out that SP as well as TBP metallacyclobutane can break up directly to form metal carbene and olefin. Thus, there is no need to assume[2c] an interconversion of one metallacycle conformation into the other before decomposition.

Symmetry Considerations of Process Feasibility. Figure 4 indicates that the formation of $L_2Mo(X)C_3H_6$ from ethylene and the metal carbene $L_2Mo(X)CH_2$ (eq 1b) has a modest activation barrier. The feasibility of this formally symmetry forbidden $[2_\pi + 2_\pi]$ addition reaction is in sharp contrast to the $[2_\pi + 2_\pi]$ addition reaction between two olefins (eq 2). The reaction in eq

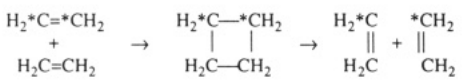

(2)

2 is symmetry-forbidden by the Woodward–Hoffmann rules,[19] and quantitative calculations have revealed an activation barrier of more than 100 kcal mol^{-1}. The barrier stems[18] from the out-of-phase interaction between the occupied π orbitals on the two approaching ethylenes ($2b_{3u}$ in Figure 6). This repulsive interaction is increased by the good overlaps between the two π orbitals as well as their degenerate energies. A transfer of two electrons from the $2b_{3u}$ orbital to the in-phase combination, $1b_{2u}$, between π^* orbitals on the two approaching ethylenes will eventually eliminate the repulsion. However, the π to π^* charge transfer cannot take place before $2b_{3u}$ and $1b_{2u}$ are of the same energy due to the lack of overlap between π and π^* orbitals on opposite ethylenes, hence the energy barrier for the process in eq 2.

We present a correlation diagram for the formation of metallacyclobutane **4** in Figure 7. The diagram correlates π- and σ-type orbitals on the reactant side with the orbitals responsible for the four bonds in the cyclic ring structure on the product side. The replacement of one ethylene by a metal carbene in the $[2_\pi + 2_\pi]$ addition reaction (eq 1)

(19) Woodward, R. B.; Hoffmann, R. In *The Conservation of Orbital Symmetry*; Verlag Chemie: Weinheim, Germany, 1970.

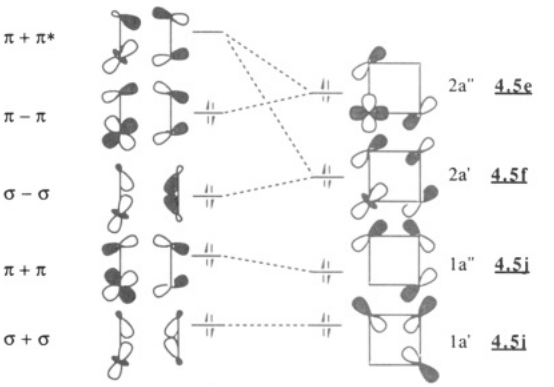

Figure 7. Correlation diagram for the reaction between the carbene and ethylene leading to the formation of the square-pyramidal intermediate **4**.

Table V. Relative Stability[a] of the SP Intermediate (ΔH_{elect}^{SP}) and the TBP Intermediate (ΔH_{elect}^{TBP}) with Respect to the Reactants $L_2Mo(X)CH_2$ Plus C_2H_4 (ΔH_{elect}^{react}) for the Reactions in Eq 1b

substituents on the metal center	$\Delta H_{elect}^{react} - \Delta H_{elect}^{SP}$	$\Delta H_{elect}^{react} - \Delta H_{elect}^{TBP}$
L = Cl, X = O	53.97	21.03
L = Cl, X = NH	43.30	37.50
L = CH_3O, X = O	66.13	44.13
L = CH_3O, X = NH	60.67	57.43
L = CF_3O, X = O	60.89	43.49
L = CF_3O, X = NH	48.52	73.86

[a] The energy differences are in kJ mol^{-1}.

introduces a substantial energy gap between the two occupied π orbitals, as π_{olefin} is 4 eV higher in energy than $\pi_{carbene}$. The energy gap will help to reduce the repulsive interaction between the two approaching π orbitals in the early stages of the $[2_\pi + 2_\pi]$ addition reaction of eq 1.

The final formation of a cyclic structure from two double bonds requires transfer of charge from the occupied π orbitals to the empty π^* orbitals. This transfer gave rise to an energy barrier for the formation of cyclobutane due to the lack of π to π^* overlaps. The π to π^* overlaps are different from zero for the reaction between olefin and metal carbene (**11c,d** and **12a,b**). The nonzero overlaps allow for a gradual and continuous transfer of charge as the cyclic structure is formed (Figure 7). The gradual transfer ensures in turn a smooth correlation without a substantial energy barrier. The donation from the π_{olefin} to the carbene acceptor orbital, $\pi^*_{carbene}$, amounts to between 0.7 and 0.8 e depending on the substituents, whereas the back-donation from the $\pi_{carbene}$ to the π^* orbital on C_2H_4 range from 1 to 0.9 e. In the TBP intermediates we found less donation from the π_{olefin} to the metal center (between 0.6 and 0.7 e) and consequently less back-donation to the π^*_{olefin} (between 0.8 and 0.9 e). Rappé[4] et al. have provided a rationale for the feasibility of the $[2\pi + 2\pi]$ addition between olefin and metal carbene based on general valence bond calculations (GVB). The language in the GVB theory is somewhat different from that employed in normal orbital arguments. However, the two-orbital–four-electron repulsions which are of crucial importance in our analysis are also recognized as key factors in the GVB analysis, where they are referred to as Pauli repulsion.

Stability of $L_2Mo(X)C_3H_6$ with Respect to C_2H_4 and $L_2Mo(X)CH_2$. In Table V, we display the calculated stability of the $L_2Mo(X)C_3H_6$ metallacycle with respect to its decomposition into $L_2Mo(X)CH_2$ and C_2H_4. The

Table VI. Calculated Relative Energies[a] of Square-Pyramidal (SP) and Trigonal-Bipyramidal (TBP) $L_2Mo(NH)C_3H_6$ in Terms of C_2H_4 and $L_2Mo(NH)CH_2$ Fragments (L = OCH_3, OCF_3)

L	$\Delta E[L_2Mo(NH)CH_2]$[b]	$\Delta E[C_2H_4]$[c]	$\Delta E_{int}^{SP} - \Delta E_{int}^{TBP}$[d]	$\Delta E_{rel}^{TBP/SP}$[e]
OCH_3	4.0	−23.9	16.7	3.2
OCF_3	21.4	−20.8	24.7	−25.3

[a] The energies are in kJ mol^{-1}. [b] $\Delta E[L_2Mo(NH)CH_2]$ = (energy of $L_2Mo(NH)CH_2$ in SP conformation) − (energy of $L_2Mo(NH)CH_2$ in TBP conformation). [c] $\Delta E[C_2H_4]$ = (energy of C_2H_4 in SP conformation) − (energy of C_2H_4 in TBP conformation). [d] ΔE_{int}^{SP} and ΔE_{int}^{TBP} are the bonding energies between the two fragments in SP and TBP. [e] $\Delta E_{rel}^{TBP/SP} = \Delta E^{TBP} - \Delta E^{SP}$ is the energy difference between the TBP and SP conformations of $L_2Mo(NH)C_3H_6$. We have $\Delta E_{rel}^{TBP/SP} = -\{\Delta E[L_2Mo(NH)CH_2] + \Delta E[C_2H_4] + [\Delta E_{int}^{SP} - \Delta E_{int}^{TBP}]\}$.

stability has been studied for different choices of L and X, and we note that the metallacycle in all cases is stable toward decomposition. The nature of the spectator ligand X has some influence on the stability of the metallacycle. Thus, square-pyramidal intermediates are calculated to be more stable with oxygen rather than NH as the spectator ligand, whereas the order of stability is reversed for the TBP conformation. The latter trend is likely related to a more destabilizing interaction in **6** for the stronger π-donor oxygen. Chlorine as a coligand is seen to produce less stable metallacycles than either of the alkoxy groups, and the square-pyramidal intermediates are in general calculated to be more stable than the TBP conformation. The only exception is $(CF_3O)_2Mo(NH)C_3H_6$, for which we find a preference for the TBP structure. The calculated switchover in the case of $(OR)_2Mo(NH)C_3H_6$ from SP for R = CH_3 to TBP for R = CF_3 is in accordance with experimental findings, in that more electron-donating alkoxy groups give rise to a SP structure whereas electron-withdrawing alkoxy ligands afford a TBP structure.

We have investigated this important crossover further in Table VI, where the relative stabilities for the SP and TBP conformations of $(L)_2Mo(NH)C_3H_6$ with L = OCH_3, OCF_3 are analyzed. The analysis is based on a Haber cycle similar to that presented in Figure 3, except that now the two fragments are ethylene and $L_2Mo(NH)CH_2$ rather than $L_2Mo(NH)$ and C_3H_6. The cycle employed in Table VI consists of four elementary steps: dissociation of the TBP metallacycle into $L_2Mo(NH)CH_2$ and C_2H_4 moieties, their transformation into the frameworks taken up in the SP geometry, interaction of the two fragments upon the formation of the SP intermediate, and finally, isomerization of an intermediate structure from its square-pyramidal conformation to the trigonal-bipyramidal one.

We calculate the $L_2Mo(NH)CH_2$ fragments to be more stable in the TBP intermediates. We note that although the shape of the $L_2Mo(NH)$ moiety in the SP metallacycle resembles that in the free carbene **2b**, this is not enough to render the carbene fragment $L_2Mo(NH)CH_2$ in the SP framework to be more stable than that of the TBP species. Instead, the relative stability of the carbene fragments in the TBP and SP structures can be related to the degree by which the Mo=C double bonds of 1.87 Å (OCH_3) and 1.89 Å (OCF_3), respectively, are being stretched on going from a free carbene to a single Mo–C_α bond in either of the intermediates. Shorter Mo–C_3 bonds of 2.059 Å (OCF_3) and 2.073 Å (OCH_3) in TBP therefore yield more stable carbene fragments than the somewhat longer Mo–C_3 bonds of 2.176 Å (OCF_3) and 2.173 Å (OCH_3) in SP. On the other hand, the ethylene fragment was found to be more stable in the square-pyramidal intermediates, where the C_1–C_2 bond distances of 1.50–1.51 Å are roughly 0.07 Å shorter than those calculated for the TBP intermediates. The interaction energy between ethylene and the metal carbene is finally seen to be most favorable in the TBP metallacycle with the shortest Mo–C_1 distance.

It is apparent from Table VI that the pivoting term of importance for the preferred conformation in $(L)_2Mo(NH)C_3H_6$ is the relative stability of the carbene fragment in the alternative SP or TBP intermediate. In the OCF_3 system too much energy (21.4 kJ/mol) is required to stretch the strong Mo–$C_{carbene}$ bond to the full length in the SP conformation. For this reason, the system adopts a TBP conformation. The TBP structure is also favored by a stronger (by 24.7 kJ/mol) interaction between ethylene and the metal carbene.

In the methoxy system, the deformation of the $(CH_3O)_2Mo(NH)CH_2$ carbene into the framework taken up in the SP structure requires only a mere 4.0 kJ mol^{-1} more than the deformation into the $(CH_3O)_2Mo(NH)CH_2$ (TBP) framework. In part, it is a result of the relatively weaker Mo–$C_{carbene}$ bond, which is easier to stretch to the length adopted in the SP structure. The calculated short olefinic carbon–carbon bond strongly favors the formation of the square-pyramidal intermediate by 23.9 kJ mol^{-1}. The interaction energy between $(CH_3O)_2Mo(NH)CH_2$ (SP) and C_2H_4 (SP) only partially counteracts the above stabilization. The end result is a preference of the SP geometry **4** over the TBP structure **3** (Table VI).

The magnitude of the thermodynamic stabilization of the ring systems, as calculated in this study, compares well with the experimental kinetic parameters[2c] for the olefin dissociation from the real-life square-pyramidal tungstacycles. Feldman et al. quoted activation enthalpies of 82.4 and 92.0 kJ mol^{-1} for the breakup of the $(ArO)_2W(NAr)[CH_2CH(t\text{-}Bu)CH_2]$ and $(O\text{-}t\text{-}Bu)_2W(NAr)[CH_2CH(t\text{-}Bu)CH_2]$ intermediates, respectively. Previous theoretical GVB studies[4a,b] dealt with olefin insertion into the Cl_2TiCH_2 carbene and obtained an activation barrier of 91.5 kJ mol^{-1} for the decomposition of the titanacyclobutane.

IV. Concluding Remarks

For the olefin exchange reactions in eq 1b, we have discussed the geometries and the relative energies of the reactants/products as well as the two cyclic intermediates with respectively square-pyramidal and trigonal-bipyramidal structures. The molybdenum carbene complexes with various coligands L (Cl, OCH_3, OCF_3) and spectator ligands X (O, NH) were used to model the real-life olefin metathesis catalysts. We have studied the relative stabilities of the two types of intermediates in terms of (i) the energies of the $L_2Mo(X)$ and C_3H_6 fragments and the interaction energy between them as well as (ii) the energies and the interaction between the $L_2Mo(X)CH_2$ and C_2H_4 fragments.

The metal carbene $L_2Mo(X)CH_2$ and ethylene can react[2c] along two alternative pathways, yielding square-pyramidal or trigonal-bipyramidal metallacycles, respectively. We have shown that the reactions under investigation shared the same path for the initial stage of the olefin attack onto the carbene molecule, all the way until a π complex (possibly a transition state), **9**, was formed. The reactions can then proceed along one of the two proposed routes. Our work demonstrates that the de-

composition of the square-pyramidal intermediate need not occur via a trigonal-pyramidal structure, as once suggested in the literature.[2b]

The present investigation finds, in accord with the experimental evidence, that electron-withdrawing coligands (OCF_3) facilitate an early nucleophilic attack of an olefinic carbon atom on the metal center, leading to the formation of a trigonal-bipyramidal intermediate. The electron-donating coligands (OCH_3), on the other hand, delay the nucleophilic attack and result in the formation of a square-pyramidal intermediate. The different timing in the two paths has been rationalized in terms of orbital interaction considerations.

We have calculated the metallacyclic systems to be more stable than the reactants/products. The calculated activation enthalpies for the decomposition of the intermediate metallacycle compare well with the experimental estimates. The reactions in eq 1b were shown to have a small electronic barrier of 10 kJ mol^{-1}.

On the basis of correlation diagrams, we have contrasted the feasibility of the organometallic $[2_\pi + 2_\pi]$ processes in eq 1b with the analogous symmetry-forbidden organic $[2_\pi + 2_\pi]$ reactions between two olefin double bonds. Organic $[2_\pi + 2_\pi]$ reactions owe their high reaction barrier to the lack of interaction between approaching π and π^* orbitals as well as a large repulsive π-to-π interaction. The repulsive interactions are enhanced further by the close energy of the π orbitals. The repulsive interactions in the organometallic reactions is reduced by a substantial energy gap between the two π orbitals involved. The organometallic reactions are further helped by substantial π to π^* overlaps.

As shown in Table VI, there is a preference for the formation of the SP intermediate $L_2Mo(NH)C_3H_6$ if L = OCH_3 and the TBP intermediate if L = OCF_3. This is in line with experimental findings in that electron-withdrawing alkoxy groups give rise to TBP structures, whereas electron-releasing groups result in SP structures. A rationale of this preference has been provided, based on the Mo–CH_2 bond strength in $L_2Mo(NH)CH_2$.

Acknowledgment. This investigation was supported by the Natural Sciences and Engineering Research Council of Canada (NSERC). We also acknowledge access to the IBM-6000/RISC facilities at the University of Calgary.

OM920474+